

Verification of Hygrothermal Simulations Using Silicone Encapsulated Climate Sensors in Continuously Operated IGBT Power Modules

Sören Fröhling^{1,2}, Benedikt Kostka¹, Johannes C. Wenzel¹, Katharina Fischer², Jan-Hendrik Peters³, Michael Hanf³, Christian Zorn², Kirsten Dehning⁴, Stefan Zimmermann⁴, Nando Kaminski³, and Axel Mertens¹

¹Institute for Drive Systems and Power Electronics, Leibniz University Hannover, 30167 Hannover Germany,
 soeren.froehling@ial.uni-hannover.de

²Fraunhofer Institute for Wind Energy Systems IWES, 30159 Hannover Germany

³Institute for Electrical Drives, Power Electronics and Devices, University of Bremen, 28359 Bremen Germany

⁴Institute of Electrical Engineering and Measurement Technology, Leibniz University Hannover, 30167 Hannover Germany

Abstract—This paper presents measurements of temperature and humidity conditions in a power module during continuous pulse-width modulation (PWM) operation. Based on the results, a developed hygrothermal simulation model is validated. This can subsequently be used later to identify critical operating conditions which can create lifetime-reducing microclimates on the chip level. This approach enables the implementation of a condition monitoring system based on the microclimate inside the power module.

Index Terms—Degradation, IGBT, Reliability, Silicone gel

I. INTRODUCTION

In various applications (e.g., wind turbines and traction drives), power electronic systems are exposed to harsh climatic conditions and yet must survive a service life of up to 30 years. Analysis of field data from more than 7,400 operating years of wind turbines indicates that climatic conditions such as humidity and temperature have an influence on the failure rate [1], [2]. The effect of humidity on converter reliability has recently been confirmed and quantified in [3]. This confirms a global trend observed also in other applications of power electronics [4], [5]. In addition to thermally induced failures of power semiconductor modules, moisture-related failures have attracted more attention in recent years. IGBT power modules are often considered as one of the main causes of moisture-related failures. Moisture causes electrochemical corrosion at the junction termination of semiconductor chips, which leads to reduced blocking capability and increased leakage current [6], [7]. The microclimate inside the housing, especially at the chip surface, is most critical in terms of moisture-driven ageing of insulation layers and corrosion of metals. With the increasing awareness of these failure mechanisms, first manufacturers

have reacted with moisture-resistant designs [8]. However, as the large majority of power semiconductor modules installed in the field is from older generations, the topic remains of primary interest for economic operation. Typically, IGBT power modules have a housing made of a polymer, i.e. they are not hermetically sealed. In addition, such power modules are filled with a silicone gel that completely covers the substrate. In general, it is possible for water molecules to penetrate through the housing and come into direct contact with the direct bonded copper substrate (DCB substrate). The silicone also provides a diffusion path and is able to store water molecules. Together with the surrounding climatic conditions in the power cabinet, these properties of the module design determine the module-internal microclimate having an influence on the lifetime of the power module. Temperature swings significantly affect the internal microclimate since the relative humidity is dependent on the absolute humidity and temperature. Furthermore, internal losses heat up the devices when the converter system is operating, therefore reducing the relative humidity in the chip areas.

This paper addresses the issue of humidity-induced failures of IGBT modules and presents measurements of the climatic conditions inside an IGBT module during operation using commercially available combined temperature-humidity sensors (RH/T sensors) encapsulated in the silicone

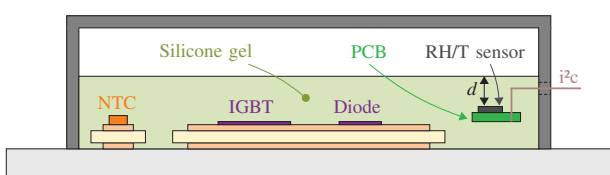


Fig. 1: Schematic diagram of the module cross-section to illustrating the sensor positions

This work is part of the project ReCoWind and was funded by the Federal Ministry for Economic Affairs and Climate Action on the basis of a decision by the German Bundestag. Grant number: 0324336A/C/E.

gel. The measurement results are then used to validate a developed hygrothermal simulation model based on Fick's diffusion laws. With information about critical operating conditions derived from the hygrothermal simulation model, it is possible to set up preventive operation management for the converter which considers the microclimate in the power module.

II. MEASUREMENT

For this work, a half-bridge module, designed for a continuous DC collector current of $I_{CDC} = 1\text{ kA}$ at a case temperature of 100°C and a rated collector-emitter voltage of $V_{CES} = 1.7\text{ kV}$, has been equipped by the manufacturer with two sensors of type SENSIRION SHT35 measuring relative humidity and temperature. The measurement data from the integrated RH/T sensors are acquired using the hardware and software available from the manufacturer of the sensors.

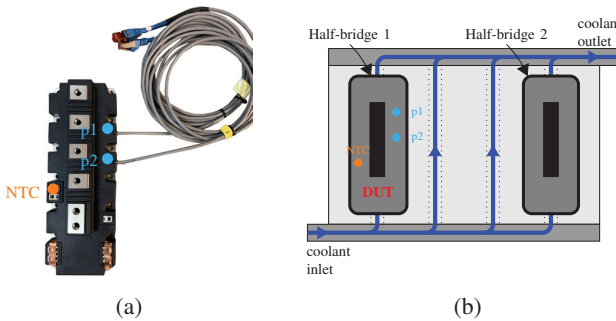


Fig. 2: Image from the device under test (DUT) with RH/T and NTC sensor positions (a) and a schematic representation of the coolant flow inside the heat sink including the two half-bridges (b)

Fig. 2 (a) depicts the sensor-equipped module. In addition to the standard NTC sensor (orange dot), the positions of the encapsulated RH/T sensors are also marked (light blue dots). As the NTC sensor, each RH/T sensor is placed inside one of the module's "side pockets", in order to give nearly the same distance to the semiconductor chips. In the housing, feed-through holes were drilled so that the signal wires of the RH/T sensors could be led out. After this, the holes were sealed with an adhesive and thus the positions of the sensors were fixed. Then the module was encapsulated with silicone under vacuum in agreement with the standard procedure for power modules. However, it cannot be excluded that there is an air inclusion between the sensitive area of the sensor and the silicone gel on top of it. Unlike the NTC sensor, the PCB equipped with the RH/T sensor must be insulated from the module's base plate, so that there is no direct (thermal) connection (see Fig. 1). This means that the sensor's temperature does not represent the base-plate temperature nor the chip temperature. Instead, it represents the temperature inside the silicone gel.

A. Measurement Setup

In the experiments carried out, a full-bridge setup consisting of two IGBT half-bridge modules (one equipped with RH/T sensors, see Fig. 2 (b)) and a load inductance L was used. The schematic circuit diagram can be found in Fig. 3. Under continuous PWM operation, a sinusoidal load current with a frequency of $f_1 = 50\text{ Hz}$ was injected into the load inductance L .

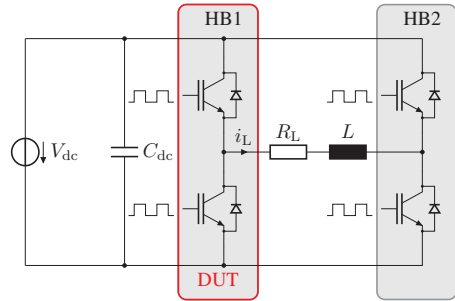


Fig. 3: Circuit diagram of the test setup for continuous PWM operation with a predominantly inductive load

The modules are mounted on a water-cooled heat sink, where the coolant intake temperature is actively controlled by the cooling system to give $T_{cool,in} = 23^\circ\text{C}$. Fig. 2 (b) shows the coolant flow inside the heat sink and depicts the positions of both half-bridge modules placed on the heat sink. Since four modules could be placed on the heat sink but only two have been used in the present experimental setup, the remaining two cooling channels between the half-bridge modules are not used (see Fig. 2 (b)). The fact that the layout is not fully symmetric and the RH/T sensors of the DUT are mounted on the right-hand side, i.e. towards the unused cooling channels; this has an impact on the measured temperature and needs to be taken into account, especially when comparing the sensor's temperature with the temperature at the module's NTC which faces away from the unused cooling channels. Furthermore, the cooling water is supplied to the fluid cooler from one end and then distributed over the entire surface of the heat sink. The heated cooling water is drained out at the other end of the heat sink. The coolant first passes the sensor p2 of the module DUT and then the sensor p1. This information is important for the later evaluation of the measurement results.

For all measurements carried out in this work, a load inductance of $L = 1.06\text{ mH}$ with an ohmic resistance of $R_L = 1.8\text{ m}\Omega$ and a switching frequency of $f_{sw} = 4.5\text{ kHz}$ are used. The DC-link voltage is kept constant at $V_{dc} = 1\text{ kV}$ while the load current is varied during the measurement, depending on the operating point (OP). The DC-link capacitance is $C_{dc} = 3.6\text{ mF}$. It should also be noted that, in this work, the load current i_L is described by its amplitude instead of its root mean square value. In accordance with the suggestions from the gate driver's manufacturer, a turn-

on gate resistance of $R_{G,\text{on}} = 1.2\Omega$ and a turn-off gate resistance of $R_{G,\text{off}} = 3.4\Omega$ are used. Tab. I summarizes the relevant parameters for the measurement setup.

TABLE I: Test setup parameters used in this work

V_{dc}	C_{dc}	L	f_{sw}	$R_{G,\text{on}}$	$R_{G,\text{off}}$	$T_{cool,\text{in}}$
1 kV	3.6 mF	1.06 mH	4.5 kHz	1.2 Ω	3.4 Ω	23 °C

In Fig. 4, the laboratory setup used is depicted and Fig. 5 shows the measured load current for two OPs with the corresponding DC-link voltage as an example.



Fig. 4: Laboratory test setup with fluid cooler and two IGBT modules, including the measurement circuitry and control peripherals

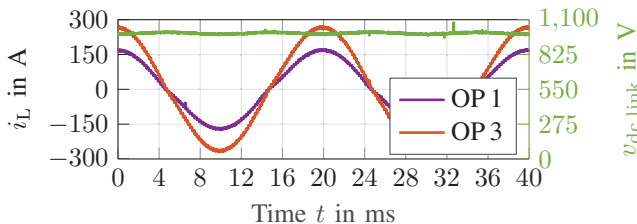


Fig. 5: Measured load current i_L and DC-link voltage v_{dc} for the operating points OP 1 and OP 3

B. Measurement Results without Electrical Load

First, using the sensor-equipped module (see Fig. 2 (a)), a calibration was performed, for which the module was subjected to a climatic stepwise change from 20 °C and 40 %RH, held for 24 h, to 40 °C and 60 %RH in a climatic chamber. It should be noted that only the module itself is in the climate chamber and is subjected to the calibration process. Influences from a cooling system are therefore not relevant here. The calibration results obtained are shown in Fig. 6. With relatively small deviations in temperature and humidity in the steady state, a reliable climate measurement using the integrated sensors can be assumed. In addition, a relatively long response time of the humidity intrusion into the silicone gel is observed, especially compared to the response time of the temperature.

The interpretation of the measured temperature and especially the humidity is an important aspect. By inserting the

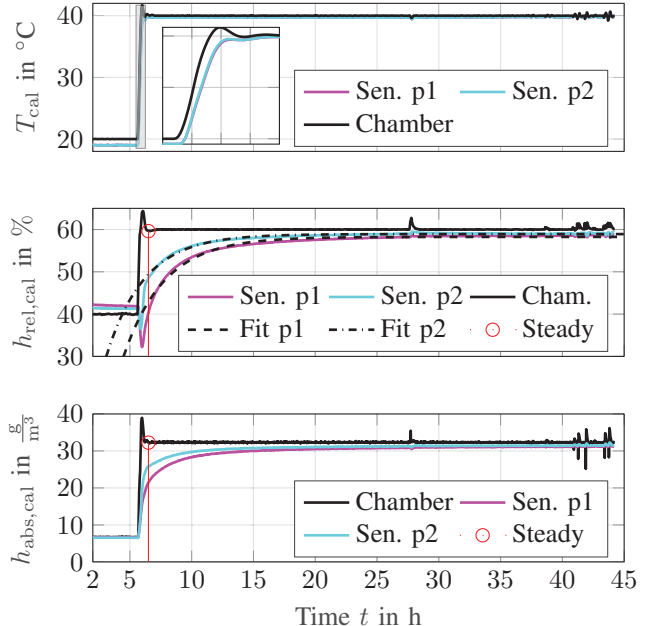


Fig. 6: Calibration data of the DUT in a climatic chamber; Climatic stepwise change from 20 °C and 40 %RH to 40 °C and 60 %RH

sensors into the silicone gel, the "system" to be measured is influenced. The sensors have a capacitive measuring element that is sensitive to the ingress of moisture, which is evaluated by the sensor. Due to this measurement method, a distinction must be made between the results of the sensor measurement and the climate actually present in the silicone gel. These two cases are not the same.

The time constant of the diffusion process for humidity is an important parameter for the interpretation and evaluation of the sensor data. This parameter can be used to identify any differences in dynamic behavior that may be due to variations in the placement of the sensors in the module. Two fit functions are used to extract the hygric time constants for the two sensors under investigation. Due to the simultaneous step changes in temperature and relative humidity, the data points relevant for the time constants can only be used after the time marked as "steady" in Fig. 6. After this point in time, the temperature has settled to a constant value so that the hygric processes can be assumed to be isothermal. Dynamic processes, such as the temporary dip of the relative humidity at the start of the rising temperature slope and also the overshoot behavior of the climate chamber thus do not have an influence.

Fig. 6 also shows the absolute humidities calculated from the dew-point curve in air (see Fig. 7). Since the absolute humidity inside the climatic chamber is nearly constant at the marked point in time "steady", it can be concluded that the recorded relative humidities from the sensors p1 and p2 are exclusively due to the diffusion of the humidity

from the climate chamber into the module at $T = 40^\circ\text{C}$. Furthermore, it should be noted that in the steady state the measured absolute humidity of the sensors p1 and p2 converge to the measured ambient absolute humidity in the climate chamber. Based on the measurement results from the calibration procedure, there must be a small air volume between the silicone gel and the sensitive element of the sensor. The level of absolute humidity in the silicone gel is higher than in the small air volume due to the higher solubility. The diffusion path of the absolute humidity is therefore from the ambient air via the silicone gel into the already mentioned small air volume at the sensor.

TABLE II: Time constants fitted to the results shown in Fig. 6 and calculated diffusion coefficient at a temperature of $T = 40^\circ\text{C}$ (D_{40})

Sensor	$\tau_{\text{h,rel}}$	D_{40}
p1	3.3 h	$2.3 \times 10^{-10} \frac{\text{m}^2}{\text{s}}$
p2	3.1 h	$2.4 \times 10^{-10} \frac{\text{m}^2}{\text{s}}$

The time constants derived from the calibration data of the sensors p1 and p2 and the respective fitted functions are listed in Tab. II. It should be noted that the obtained time constants are valid under the conditions of the specific test environment, since the temperature present during the diffusion process has a significant influence.

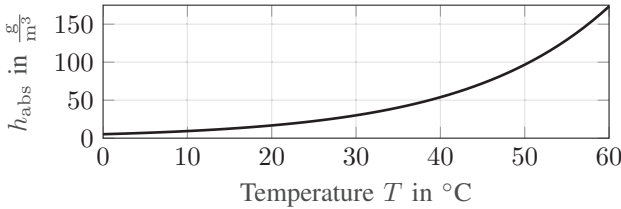


Fig. 7: Utilized dew-point curve in air. Fit function based on data from [9]

Knowledge of the diffusion coefficient D is important for the diffusion process to be simulated. With the aid of the time constant $\tau_{\text{h,rel}}$ extracted from the calibration data, a diffusion coefficient can be determined which is approximately valid for a temperature of 40°C . Here, the diffusion process of water molecules from the air (gas) through the silicone gel into the small air volume at the sensor is considered. The diffusion length d is another crucial parameter. The module housing of the power semiconductor is not completely sealed at the top due to the power terminals leading out of the module. Since a significantly greater diffusion coefficient can be assumed in gases than in solids, the dominant diffusion length d is assumed to be the layer thickness of the silicone above the RH/T sensor (see Fig. 1). In general, the specification of a diffusion length is still only a simplifying assumption since different materials are

found in the diffusion path. Furthermore, the diffusion length cannot be attributed to a single path. For example, an influence of the diffusion path from the environment through the polymer housing of the module to the sensor is to be expected. In [10], an approach is shown for which, in the case of Fick's diffusion, the diffusion coefficient D can be calculated using the 95 % saturation level $\tau_{0.95} = 3 \cdot \tau_{\text{h,rel}}$:

$$D = \frac{-d^2}{\tau_{0.95} \cdot \pi^2} \cdot \ln \left(\frac{8}{\pi^2} (1 - 0.95) \right) \quad (1)$$

The results for the diffusion coefficients D_{40} at a temperature of 40°C for the two RH/T sensors are listed in Tab. II. It should be noted that this calculation method is only a rough approximation for the case under consideration. Compared to the diffusion coefficients given in the literature for common gases, fluids, and solids, and with regard to the diffusion length present, the diffusion coefficients determined are in a realistic range.

C. Measurement Results with Electrical Load

Fig. 8 shows the obtained results, for which different OPs have been applied by means of the set current. In addition, the temperature of the module's NTC sensor T_{NTC} is depicted at the end of OP 1 and OP 3. Furthermore, Tab. III summarizes the climatic conditions at the encapsulated sensors (p1 and p2) at the end of each OP tested.

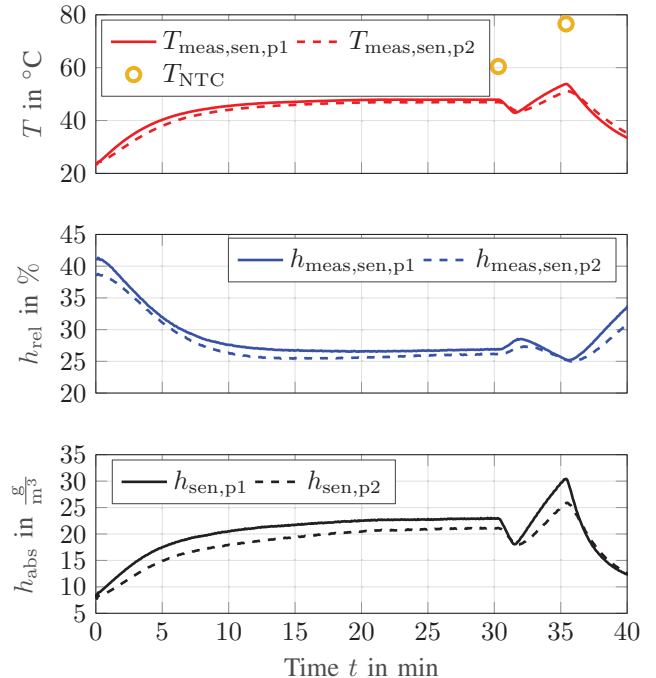


Fig. 8: Obtained relative humidity and temperature for the module equipped with the sensors. In addition, the curves of the absolute humidity, based on the dew-point curve in air, are shown.

TABLE III: Corresponding load profile to the results of Fig. 8 including the load current \hat{i}_L , the duration of each approached OP, the calculated power losses P_{loss} and the final climatic values of the encapsulated sensors

OP	Duration	Load current \hat{i}_L	Final values sensor p1	Final values sensor p2	Power losses P_{loss}
1	30 min	170 A	48 °C, 27 %RH	47 °C, 26 %RH	52.3 W
2	1 min	0 A	43 °C, 29 %RH	43 °C, 27 %RH	0 W
3	4 min	270 A	54 °C, 25 %RH	51 °C, 25 %RH	84.2 W
4	5 min	0 A	33 °C, 34 %RH	35 °C, 31 %RH	0 W

At the beginning, the temperature and relative humidity corresponds to typical indoor conditions. First, a load current of 170 A (OP 1) is applied for 30 min, causing the temperature of both sensors to rise with PT₁ behavior until it reaches a steady-state value after approximately 15 min. In contrast, the relative humidity falls with rising temperature in the first 15 min. However, in the last 5 min at OP 1, the relative humidity at both sensors increases as the temperature rises, or remains constant.

The small difference of 1 K in the final values of the measured temperature is most likely due to the different positions of the sensors, as sensor p2 is closer to the coolant inlet and therefore the coolant under sensor p1 has already been heated up slightly. Different thermal coupling between the sensors and the base plate could also play a role, as the sensors have no direct connection to the base plate. Comparing the temperatures of the sensors p1 and p2 with the measured NTC temperature at 30 min reveals a difference in the measured temperatures of approx. 12 K. In contrast to the encapsulated sensors p1 and p2, the NTC is directly connected to the DCB, resulting in a better thermal coupling with the base plate and chips and thus in a higher temperature at the NTC.

After 30 min at OP 1, the load current is set to zero (OP 2) for 1 min. At both sensors, the temperature drops and the relative humidity increases. The temperature at sensor p1 drops faster than at sensor p2, indicating that the thermal coupling of sensor p1 to the base plate, and thus to the heat sink, is better than that of sensor p2.

Subsequently, a load current of 270 A is applied for 4 min (OP 3), which leads to an increasing temperature and a decreasing relative humidity. Again, the transient response of sensor p1 is faster than that of sensor p2, which is in good agreement with the results previously obtained for OP 1 and OP 2. The temperature of the NTC at the end of OP 3 is $T_{\text{NTC}} \approx 77^\circ\text{C}$, resulting in a differences of 23 K from sensor p1 and 26 K from sensor p2, respectively.

Finally, the load current is set to zero (OP 4) again for 5 min, resulting in decreasing temperatures and rising relative humidities at both sensors.

In addition Fig. 8 shows the calculated absolute humidity (h_{abs}) by using the dew-point curve for air (see Fig. 7) and the obtained measurement results (h_{rel} and T) during PWM operation. Obviously, the calculated absolute humidity fluctuates strongly with the measured temperatures. Such dy-

namic changes of the absolute humidity are not exclusively due to diffusion processes from the ambient air to the sensor, since the ambient climate does not change significantly. This is also confirmed by the determined time constants from the calibration measurement (see Tab. II). Furthermore, it can be assumed that the DUT has acclimatized to the ambient conditions before the measurements, due to a long storage period in the laboratory. Instead, the temperature dependence of the solubility of the water molecules in air and silicone becomes clear here. Due to the air volume directly at the sensor, an interface between the silicone gel and the air volume exists. At such interfaces, concentration steps occur caused by the different solubilities of the materials [11].

The temperature dependence of the solubilities of water in air [12], [13] and water in silicone [14] is shown in Eq. 2. $M_w = 18.02 \text{ g/mol}$ is the molar mass of water, $R_0 = 8.314 \text{ J/molK}$ is the universal gas constant, ΔH_s is the enthalpy and S_0 is the solubility constant. Using the silicone gel parameters $\Delta H_s = -26.8 \text{ kJ/mol}$ and $S_0 = 4.12 \times 10^{-12} \text{ mg/mm}^3\text{Pa}$ from [14], it can be seen that the solubility of water in silicone gel has a much greater temperature dependence than the solubility of water in air.

$$S_{\text{air}} = \frac{M_w}{R_0 T} \quad S_{\text{sil}} = S_0 \cdot \exp\left(-\frac{\Delta H_s}{R_0 T}\right) \quad (2)$$

This effect will be explained with the help of Fig. 9: If a constant temperature distribution is initially assumed in the steady state (solid lines at $t = t_0$), moisture concentration steps occur at material interfaces in the steady state due to material-dependent solubilities, as shown here exemplary for the transition from silicone to air. If a temperature change occurs at the time $t = t_1$ (dashed lines, for example caused by power dissipation at the semiconductor), the solubility shift in both materials, which reacts with different intensity to temperature changes, also leads to partially different ΔS at material interfaces (here: $\Delta S_{\text{sil}} \gg \Delta S_{\text{air}}$). This in turn leads to moisture diffusion J_D right at the material interfaces, heading towards the air. With the fact that the RH/T sensor measures in a small air volume (visualised by the small dark blue zone), a changing absolute humidity $\Delta h_{\text{abs,sen}}$ is registered with almost the dynamics of the temperature changes, whereas the absolute humidity in the rest of the silicone gel shows no change yet due to the much higher time constants of the diffusion of moisture. The total air volume shown in Fig. 9 only serves to visualise the

characteristics for larger air volumes. Moreover, the self-heating of the semiconductors during PWM operation leads to spatial temperature gradients in the power module, this leads locally to different solubilities and concentrations of water molecules. In particular, this means that no direct statement on the absolute humidity inside the silicone gel itself is possible with the presented measurements unless the solubility of the silicone and the air is known and included in a suitable simulation model.

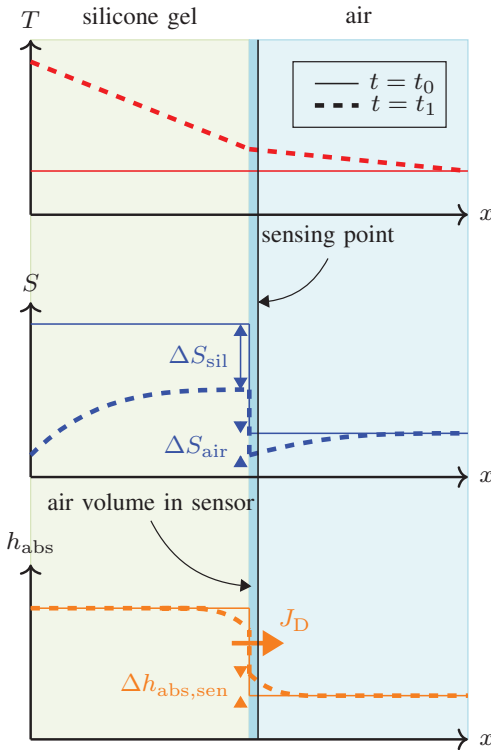


Fig. 9: Effect of temperature and different solubilities at interfaces on the measured absolute humidity at the sensor.

III. CALCULATION OF POWER LOSSES

The loss distribution over all single IGBT chips is assumed to be symmetric. The same assumption is made for the diodes. According to [15], the power losses per IGBT and diode in a full-bridge setup (see Fig. 3) can be calculated as follows:

$$P_{\text{loss}} = \frac{1}{n} \cdot (P_{c,T} + P_{c,D} + P_{sw,T} + P_{sw,D}) \quad . \quad (3)$$

The power losses per switch (P_{loss}) are the sum of the IGBTs' switching ($P_{sw,T}$) and conduction losses ($P_{c,T}$) and the switching and conduction losses of the free-wheeling diodes ($P_{sw,D}$, $P_{c,D}$) divided by the number of semiconductor pairs n (IGBT and diode) used for one switch in the module.

The conduction losses of the IGBT and diode are given by the following equations:

$$P_{c,T} = \frac{V_{0,T} \cdot \hat{i}_L}{2\pi} \cdot \left(1 + \frac{M\pi}{4} \cdot \cos \varphi\right) + \frac{r_{0,T} \cdot \hat{i}_L^2}{2\pi} \cdot \left(\frac{\pi}{4} + \frac{2M}{3} \cdot \cos \varphi\right), \quad (4)$$

$$P_{c,D} = \frac{V_{0,D} \cdot \hat{i}_L}{2\pi} \cdot \left(1 - \frac{M\pi}{4} \cdot \cos \varphi\right) + \frac{r_{0,D} \cdot \hat{i}_L^2}{2\pi} \cdot \left(\frac{\pi}{4} - \frac{2M}{3} \cdot \cos \varphi\right), \quad (5)$$

where $V_{0,T}$ is the forward bias threshold voltage of the IGBT and $V_{0,D}$ that of the diode, respectively. $r_{0,T}$ and $r_{0,D}$ are the differential resistances of the IGBT and diode. These values can be obtained from the module's datasheet. M describes the modulation index and $\cos \varphi$ is the power factor, which are dependent on the test setup (see Tab. I).

The switching losses of the IGBTs and diodes are calculated as follows:

$$P_{sw,T} = \frac{f_{sw}}{\pi} \cdot (E_{on} + E_{off}) \cdot \frac{V_{dc}}{V_{ref}} \cdot \frac{\hat{i}_L}{I_{ref}}, \quad (6)$$

$$P_{sw,D} = \frac{f_{sw}}{\pi} \cdot E_{rr} \cdot \frac{V_{dc}}{V_{ref}} \cdot \frac{\hat{i}_L}{I_{ref}} \quad . \quad (7)$$

The turn-on and turn-off switching energies of the IGBT are given by E_{on} and E_{off} , respectively. E_{rr} is the reverse-recovery energy caused by the reverse-recovery charge of the diode. Since these values, given on the module's datasheet, only apply to a specific rated voltage (V_{ref}) and rated current (I_{ref}), the obtained values have to be scaled according to the actual values used in the laboratory setup (\hat{i}_L and V_{dc}). In Equations (6) and (7), a linear dependency of the switching energy with the current and voltage applied is assumed.

Tab. III lists the calculated losses for each approached OP.

IV. SIMULATION

A. Simulation Model

The measurements presented in Section II are to be replicated by means of computer-aided simulations. In order to realistically represent humidity within power electronic components, a simulation model must be able to represent both humidity and temperature to include different load profiles, as in the measurement shown in Fig. 8. The diffusion models used here are implemented in a MATLAB script and can map the geometries considered in two dimensions. This is done on the basis of Fick's diffusion equations. As can be seen in the following, this requires the diffusion coefficient $D(T)$:

$$\frac{\partial c}{\partial t} = D(T) \cdot \left(\frac{\partial^2 c}{\partial x^2} + \frac{\partial^2 c}{\partial y^2} \right) \quad (8)$$

with

$$D(T) = D_0 \cdot \exp \left(-\frac{Q}{k \cdot T} \right) \quad (9)$$

In the above equations, the concentration c can also be interpreted as the absolute humidity h_{abs} . D_0 is the diffusion constant of one specific material, k is the Boltzmann constant, and Q is the activation energy of water.

For the temperature T , a separately executed thermal model is developed. This results in a simulation structure as shown in Fig. 10. The thermal model is implemented using the following equation:

$$\frac{\partial T}{\partial t} = -\frac{\partial J_{T,x}}{\partial x} - \frac{\partial J_{T,y}}{\partial y} = a \cdot \left(\frac{\partial^2 T}{\partial x^2} + \frac{\partial^2 T}{\partial y^2} \right) \quad (10)$$

Where a is the thermal diffusivity and can be calculated as $a = \lambda / (\rho \cdot c_p)$. J_T is the heat flux, ρ is the material-dependent density, λ is the coefficient of thermal conductivity, and c_p is its specific heat capacitance per unit mass. If the thermal diffusion is combined with the following equation describing a specific heat flux

$$\frac{P_{\text{loss}}}{A} = \dot{q} = -\lambda \cdot \left(\frac{\partial T}{\partial x} + \frac{\partial T}{\partial y} \right) \quad (11)$$

within a material, the result is a differential equation for heat transfer that is dependent on the power dissipation

$$\frac{\partial T}{\partial t} = a \cdot \left(\frac{\partial^2 T}{\partial x^2} + \frac{\partial^2 T}{\partial y^2} \right) + \frac{P_{\text{loss}}}{\rho \cdot c_p \cdot \Lambda} \quad . \quad (12)$$

Here the volume is Λ . Thus, it is possible to mathematically incorporate changes in the losses of the electrical components due to load fluctuations. To do this, it is necessary to calculate the resulting conduction and switching losses within the semiconductors as functions of the varying current, as presented in Section III.

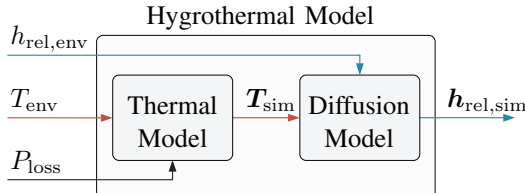


Fig. 10: Structure of the hygrothermal simulation model with weak thermal coupling. The known input parameters of the environment and load can be used to predict the humidity and temperature within the module.

Further information concerning the approach used to simulate humidity in power electronic components can be found in [16]. In the following, attention will be paid to the discretization approach used here and the simplifications assumed for the hygrothermal simulation of the module.

The modules used in the previously presented measurements were modeled as two-dimensional cross-sections, as shown in Fig. 11 (a), in both the humidity simulation model and the thermal simulation model (combined, these form the so-called hygrothermal model). The cross-section was chosen to include both an IGBT and a diode of the same half-bridge.

The discretization of the two simulated dimensions x and y can be scaled variably within the simulation structure, whose dimension has an immense influence on the simulation time. It has been shown that the diffusion equations for

absolute humidity and temperature (Eq. (8) and (10)) already provide sufficiently accurate results for thermal and humidity diffusion, solely by directly comparing two adjacent spatial positions. This can be explained more vividly using the example of the temperature distribution in the x direction shown in Fig. 11 (a): a 5×5 mesh is illustrated, whose spatial values are determined solely at the points indicated by crosses. This schematic represents exactly the geometry and the mesh that was applied for the simulation models used for this paper. If the temperatures of two adjacent crosses are unequal ($dT/dx \neq 0$), a heat flow will result, respecting the factor a . If there are n different materials between the crosses $x_{1,3}$ and $x_{2,3}$, i.e., along the path marked in red, the temperature curve resulting in one time step is assumed to be approximately linear. This is shown by the dashed line in Fig. 11 (b) in comparison to the more accurate temperature profile (solid line) with a short-term constant heat flux \dot{q} within one time step dt . In order to take into account the materials neglected in such a coarse mesh, the heat flux is included and the thermal diffusivity is weighted over the length as follows:

$$J_{T,x} = -dT \cdot \left(\sum_{i=1}^n \frac{l_{i,x}}{a_i} \right)^{-1} \quad (13)$$

Equation (10) can then be used with the resulting J_T and total dx as the sum of all $l_{i,x}$ between two mesh points. This results in the temperature change within one simulation time step or in an increase or decrease in absolute humidity for the same approach for the calculation of moisture diffusion via Equation (8). It should be noted at this point that due to varying solubilities, different moisture concentrations occur across material boundaries in the steady state, which must be taken into account in the results of moisture diffusion simulations.

B. Simulation Results

The sensor encapsulated in the silicone gel is reproduced within the simulation by using a discrete spatial value logged throughout the simulation time (two red crosses $x_{3,3}$ and $x_{4,3}$ in Fig. 11 (a)) and the assumption that the sensor represents a small volume of air inside the silicone gel.

First, the calibration measurements from the climate chamber in Fig. 6 are reproduced. For this purpose, the ambient air in the simulation is set with the measured climate values from the chamber interior for each simulation step (boundary conditions). The results can be seen in Fig. 12. In the top graph, the dashed line represents the simulated results of the temperature from the RH/T sensor. Several factors lead to such a successful result: Firstly, that the actually measured climate chamber temperature profile was included in the simulation. Secondly, all thermal conductivity parameters of the materials used could be taken from the literature. However, this does not apply to the air inside the chamber, as the heat transfer coefficient depends on the unknown flow

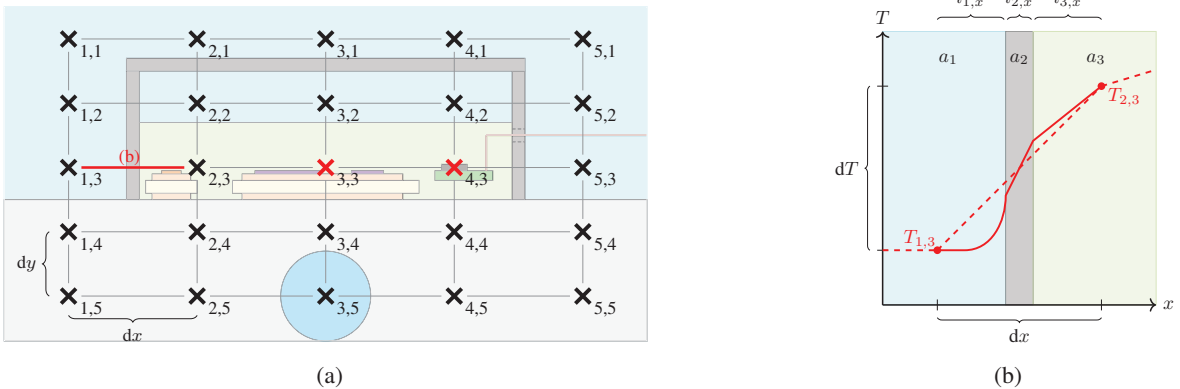


Fig. 11: 5×5 mesh discretization of the considered geometry (a) and an example simulation path between two adjacent mesh points in the x -direction through different materials (b).

velocity of the air. This parameter left some room to adjust the simulation to the measurement.

The lower graph of Fig. 12 shows the hygric model part. The dashed line again represents the results at the RH/T sensor location. Since the measurement results of the sensors (the recalculated absolute humidity), as described in Section II-C, do not allow exact conclusions about the actual moisture contained in the silicone gel during rapid temperature changes, diffusion was modeled in this case from the constant temperature of 40°C onwards. The diffusion coefficient D_{40} calculated above is used for this purpose.

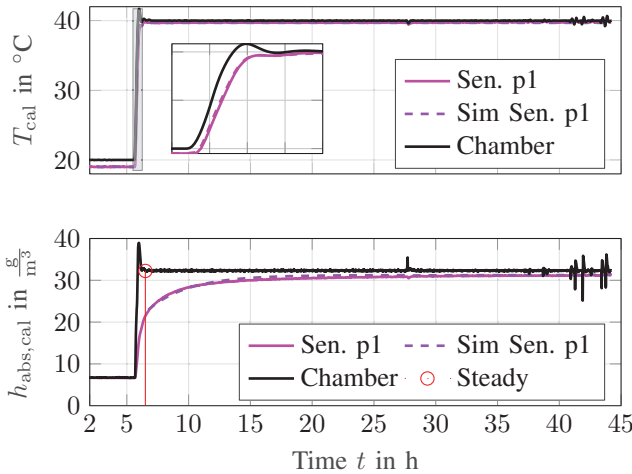


Fig. 12: Comparison of the measured calibration data with the results from the simulation for sensor p1

Fig. 13 shows the simulation results corresponding to the same scenario used to acquire the measurement results under electrical load shown in Fig. 8, and compares the measurement and simulation additionally with the simulated chip temperature. It turns out that the heat transfer coefficient for still air assumed for Fig. 12 must now be decreased by a factor of about 5 in order to reproduce the measurements

correctly. This is due to the fact that the air inside a climate chamber is circulated by a fan, which is not the case with the measurement shown in Fig. 8.

The black dashed line represents the temperature curve of the IGBT chip, which reproduces the resulting temperatures due to the varying currents. The red dashed line shows the temperature calculated over the simulation time of 40 min at the red mesh point $x_{4,3}$ marked in Fig. 11 (a). This again corresponds approximately to the sensor position in the DUT module.

The fact that the flow velocities of the two fluids present in the simulation model (cooling water and ambient air) are not known leaves some room for improvement for the variables of the heat transfer coefficients, which again makes it possible to fit the simulated temperature very accurately to the measured one.

The temperature-dependent solubility change will also cause a different absolute humidity in the silicone gel during the PWM measurement, especially at material interfaces, despite the constant ambient conditions. However, since this effect has not yet been implemented in the hygric model, no new insights can be obtained from the diffusion simulation for this scenario yet.

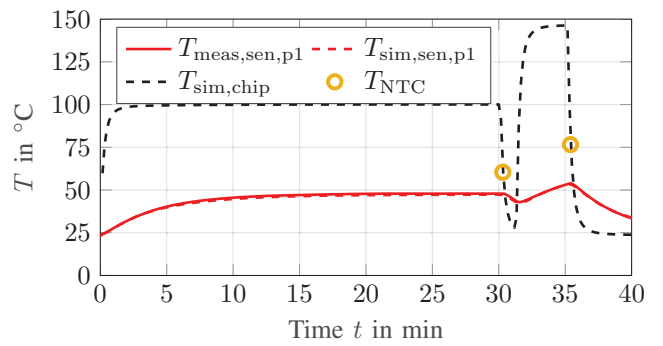


Fig. 13: Comparison between simulation and the results of the hygrothermal model for the RH/T sensor at position p1.

V. CONCLUSION & OUTLOOK

For this work a standard IGBT power module has been equipped with commercially available RH/T sensors by the manufacturer, in order to enable the measurement of climatic conditions inside the module, (i.e. relative humidity and temperature) during varying climatic and electrical load conditions. First, the climatic step response of the encapsulated sensors to varying ambient conditions has been characterized. The results reveal that the response time of temperature is negligible compared to the intrusion time of moisture from the ambient air into the module (i.e. into the silicone gel). This proves that the climatic conditions (in particular the absolute humidity) inside the power module do not necessarily match fluctuating ambient conditions.

Afterwards, the equipped module has been subjected to continuous PWM operation in a full-bridge configuration. The experimental results show that online measurement of climatic conditions in IGBT modules during continuous PWM operation is possible using commercially available sensors. When mounting and integrating RH/T sensors within a power module, there are a number of important factors to consider, which have been outlined in this paper. The sensors must be positioned before potting with silicone gel. The supply and data leads must be routed through the module's housing or appropriate terminals must be provided. Calibration of the sensors due to installation uncertainties is also necessary to obtain reliable measurements. In any case, this is a sophisticated and invasive method.

The measurement data from the RH/T sensors has provided conclusive results during continuous operation. The absolute humidity measured by the sensors is highly temperature dependent. This effect can be explained with the temperature dependence of the solubility at the material interface of air and silicone gel. Continuing on this finding, an analogy can be formulated for the DCB substrate and semiconductors. It is important to note that the material interfaces from the surface of the DCB substrate or semiconductor to the silicone gel will be decisive. These are probably not ideal. The surface of the substrate has a relatively complex shape due to the many material layers and contacts (bonding wires, corners and edges etc.), so that small air pockets could also exist between the silicone gel and the substrate. In analogy to the very dynamic and strongly temperature-dependent behavior shown by the measurement results of the absolute humidity in Section II-C, a similar behavior can be assumed at the surface of the substrate.

Based on the measurements carried out, a developed hygrothermal simulation model was presented and validated with the measured data. The validation of the simulation model has shown the importance of some physical parameters, such as the diffusion coefficient and the heat transfer coefficient of the heat sink. Most importantly, the investigations have shown that the modeling approaches using only temperature-dependent Fick's diffusion laws in the hygric

simulation model are not capable to represent the measured effects during highly dynamic temperature changes sufficiently. The solubilities of the different materials (i.e. silicone gel and air) and their temperature dependencies are decisive for the emulation of the RH/T sensor measurement data. Moreover, it is essential to model the RH/T sensor in a small air volume. This is because the material interface between the small air volume and the silicone gel is crucial for the dynamic and strongly temperature-dependent changes in absolute humidity that the sensor captures.

ACKNOWLEDGMENT

Special thanks to INFINEON TECHNOLOGIES AG for providing the semiconductor modules investigated.

REFERENCES

- [1] K. Fischer et al., "Reliability of power converters in wind turbines: Exploratory analysis of failure and operating data from a worldwide turbine fleet," *IEEE Trans. Power Electron.*, vol. 34, no. 7, pp. 6332–6344, Jul. 2019.
- [2] K. Fischer, M. Steffes, K. Pelka, B. Tegtmeier and M. Dörenkämper, "Humidity in Power Converters of Wind Turbines—Field Conditions and Their Relation with Failures," *Energies*, vol. 14, no. 7, p. 1919, 2021.
- [3] K. Pelka and K. Fischer, "Field-data-based reliability analysis of power converters in wind turbines: Assessing the effect of explanatory variables," *Wind Energy*, 2022.
- [4] C. Zorn, N. Kaminski and M. Piton, "Impact of Humidity on Railway Converters", PCIM Europe 2017, pp. 715-722, 2017
- [5] O. Schuster, A. Nagel and B. Laska, "Observation and simulation of dynamic humidity in power converters for railway applications due to moisture diffusion in plastics," in 2021 23rd EPE'21 ECCE Europe, Ghent, Belgium, 2021.
- [6] C. Zorn and N. Kaminski, "Acceleration of temperature humidity bias (THB) testing on IGBT modules by high bias levels," in Proc. IEEE 27th Int. Symp. Power Semicond. Devices IC's, 2015, pp. 385–388.
- [7] C. Papadopoulos, B. Boksteen, G. Paques, C. Corvasce, "Humidity Robustness of IGBT Guard Ring Termination," PCIM Europe 2019.
- [8] J.-H. Peters, M. Hanf, S. Clausner, C. Zorn and N. Kaminski, "Improved HV-H3TRB robustness of a 1700 V IGBT chip set in standard power modules," *Microelectronics Reliability*, vol. 126, 2021.
- [9] N. E. Daidzic, "On moist air and dew points", IJAAA (International Journal of Aviation, Aeronautics, and Aerospace), 2019.
- [10] K.M.B. Jansen, M.F. Zhang, L.J. Ernstm D.-K. Vu and L. Weiss, "Effect of temperature and humidity on moisture diffusion in an epoxy moulding compound material", *Microelectronics Reliability*, Volume 107, 2020.
- [11] S. Yoon, B. Han, and Z. Wang, "On Moisture Diffusion Modeling Using Thermal-Moisture Analogy." *ASME. J. Electron. Packag.*, 2007
- [12] X.J. Fan, E. Suhir, "Moisture Sensitivity of Plastic Packages of IC Devices", Springer New York, 2010
- [13] R. Bayerer, M. Lassmann and S. Kremp, "Transient Hygrothermal-Response of Power Modules in Inverters—The Basis for Mission Profiling Under Climate and Power Loading," in *IEEE Transactions on Power Electronics*, Jan. 2016
- [14] K. Hatori, K. Nakamura, W. Noboru, N. Soltau and E. Wiesner, "Humidity Absorption Behavior of Silicone Gel in HVIGBT Modules," 2021 23rd EPE'21 ECCE Europe, Ghent, Belgium, 2021
- [15] R. Yapa, A.J. Forsyth and R. Todd, "Analysis of SiC technology in two-level and three-level converters for aerospace applications.", 7th IET International Conference on PEMD, 2014.
- [16] J. C. Wenzel and A. Mertens, "System Level Simulation of Moisture Propagation and Effects in Wind Power Converters," 2022 24th EPE'22 ECCE Europe, 2022